Appl. Phys. B 74, 197–206 (2002)
DOI: 10.1007/s003400200794

Applied Physics B
Lasers and Optics

E. GOULIELMAKIS[1]
G. NERSISYAN[1,*]
N.A. PAPADOGIANNIS[1,2]
D. CHARALAMBIDIS[1,2]
G.D. TSAKIRIS[3,✉]
K. WITTE[3]

A dispersionless Michelson interferometer for the characterization of attosecond pulses

[1] Foundation for Research and Technology – Hellas, Institute of Electronic Structure & Lasers, Laser and Applications Division, P.O. Box 1527, 71110 Heraklion, Crete, Greece
[2] Department of Physics, University of Crete, P.O. Box 2208, 71003 Voutes-Heraklion, Greece
[3] Max-Planck-Institut für Quantenoptik, 85748 Garching, Germany

Received: 12 October 2001/
Revised version: 17 December 2001
Published online: 7 February 2002 •

ABSTRACT A novel application of a free-standing transmission grating as a beam splitter in a Michelson-type interferometer is described. The arrangement can operate in the XUV and soft X-ray spectral region and, therefore, it is well suited for the characterization of attosecond pulses. Using ray-tracing codes, we have analyzed three different setups in which spherical mirrors are employed in conjunction with the transmission grating and have investigated in detail their dispersive characteristics. It is shown that such an arrangement can be made to exhibit group-delay dispersion of ~ 1 as^2 while it provides two co-propagating and converging beams.

PACS 42.60.By; 42.65.Re; 42.65.Ky

1 Introduction

The conjecture of producing a train of attosecond pulses using high-order harmonic generation (HHG) was put forward almost 10 years ago [1, 2]. More recently, detailed theoretical investigations have confirmed this possibility and shown that it is indeed conceivable to generate a train of attosecond pulses or even a single attosecond pulse. The method utilizes the coherent properties of the high harmonics produced in the interaction of laser light with atoms in a manner analogous to the short-pulse production in mode-locked lasers [3–6]. Nonetheless, it is only now that experimental evidence has started accumulating, indicating that the femtosecond barrier towards attosecond pulses might have fallen. Attosecond beating resulting from the superposition of high harmonics obtained by focusing a femtosecond laser pulse in a gas jet has been experimentally observed [7, 8]. Furthermore, the observation of single X-ray pulses ~ 650 as in duration has been recently reported [9, 10]. The challenging problem is to find a measuring technique that unequivocally verifies the existence of attosecond pulses. In this paper, we describe such a technique, which appears to represent a viable solution to the problem of attosecond-pulse characterization.

✉ Fax: +49-89/32905-200, E-mail: tsakiris@mpq.mpg.de
*_Permanent address:_ Institute for Physical Research, Armenian National Academy of Science, Ashtarak-2, Armenia

In principle, one should be able to apply the well-known techniques from femtosecond-pulse metrology, like successive optical auto-correlations of increasing order [11, 12] to obtain the answer, i.e. characterize the attosecond pulse and ultimately measure its exact duration. The difficulty arises from the fact that, in contrast to femtosecond pulses, the attosecond pulses are necessarily in the UV–XUV spectral range and they are orders of magnitude weaker and spectrally much broader. The wavelength region below 100 nm is notoriously the most difficult spectral region to handle experimentally. It is characterized by a complete lack of refractive optical components, and even reflective optics is either of low reflectance or narrow bandwidth. However, the most demanding requirement which an attosecond measuring arrangement has to fulfill is that of almost dispersionless operation [13]. The various components of a measuring technique introduce perturbations in the quantity to be measured, namely the pulse duration, thus falsifying the results. For example, even a 5-fs pulse passing through a 1-mm-thick fused-silica plate suffers a fourfold temporal broadening. The problem becomes exceedingly more acute in dealing with sub-femtosecond pulses.

The temporal characterization of ultra-short pulses requires the use of at least second-order auto-correlation and hence of a non-linear detector with sufficient bandwidth and sensitivity. In the case of femtosecond pulses with frequencies in the visible spectral region, an amplitude-splitting interferometer (Michelson or Mach–Zehnder) in conjunction with a second-harmonic crystal is commonly used [11]. Both basic components, interferometer and detector, have to be appropriately modified or adapted for operation in the XUV spectral region. In this report, we have considered the prospect of devising a beam-splitting interferometer using a free-standing transmission grating, adapted for operation in the 10–100 nm spectral region and, therefore, ideally suited for the temporal characterization of attosecond pulses. In conjunction with focusing mirrors, this interferometer can be made to exhibit dispersion characteristics that allow measurement of pulses with a few attoseconds duration. In addition, it provides the possibility to single out either one or a group of harmonics. Although the second component needed, the non-linear detector, has yet to be found, an alternative approach [14] involving the cross-correlation technique is discussed and the applicability of the grating interferometer presented here is investigated.

2 The transmission-grating interferometer

The idea of utilizing a grating as a beam splitter in an interferometer is rather old. The natural splitting of an incident beam through dispersion has been exploited in a scheme in which the two first orders are superposed with the zeroth order by an imaging lens to give rise to an interference pattern [15]. More specifically, a Michelson interferometer based on a reflection grating, which combines the first order with the zeroth order in a double reflection off the grating, is described in [16]. The extension of this technique to the XUV spectral range can be easily accomplished by using a normal- or grazing-incidence grating. Given that the efficiency of the reflection gratings varies strongly over the range of interest, it is advantageous to use instead a transmission grating.

The concept is depicted in Fig. 1, where the transition from the conventional Michelson interferometer to the grating interferometer is schematically shown. Both interferometers split and recombine the incident beam into two co-propagating beams and they provide the possibility of delaying one beam relative to the other by translating one of the mirrors. The beam splitter normally used for wavelengths in the visible region consists of a metallic layer on a glass substrate. The option of using something similar in the region of interest, i.e. in the XUV, is precluded as all materials are opaque to this radiation. The function of the beam splitter is undertaken now by a free-standing transmission grating as shown in Fig. 1b. A monochromatic beam incident on the grating is diffracted into one zeroth order and two first orders (for simplicity, only one is shown in Fig. 1). Two mirrors reflect the zeroth order and one of the first orders straight back through the grating. In the second passage through the grating, the first order of the primary zeroth order automatically propagates in the same direction as the zeroth order of the primary first order. Because of the equal number of dispersions into the first and zeroth orders involved, the splitting of the original beam in the two arms of the interferometer is exactly 50% independently of the efficiency of the grating. The transmission-grating interferometer exhibits an additional feature, namely it spectrally analyzes the incident radiation. This property is especially desirable in case of gas harmonics produced by relatively long laser pulses where the spectrum is discrete. Then, the isolation of a single harmonic or a group of harmonics can be easily implemented by simple geometrical obstacles like apertures or knife-edges.

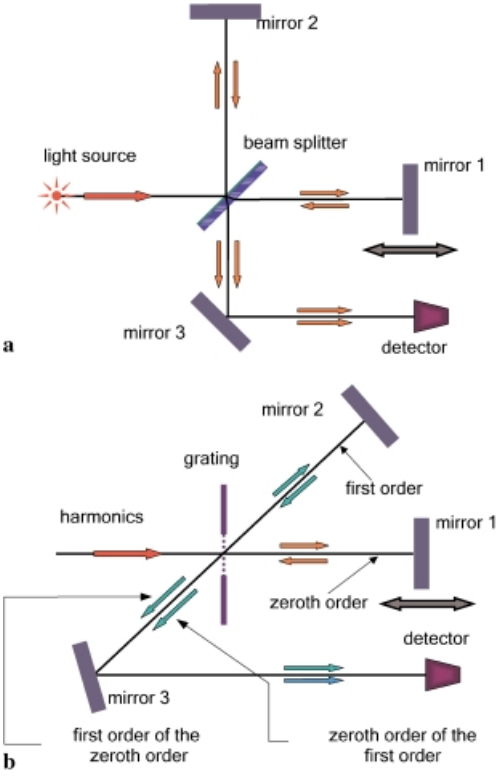

FIGURE 1 **a** The conventional Michelson interferometer used for the characterization of femtosecond pulses in auto-correlation techniques. **b** The extension of the Michelson interferometer for operation in the XUV spectral range using a free-standing transmission grating as a beam splitter. In contrast to the conventional Michelson interferometer where the mirror 3 is dispensable, in this case mirror 3 is spherical and plays a decisive role in reducing the overall dispersion of the setup to acceptable limits

In order for this technique to work with attosecond pulses, the grating and mirror configuration must be truly free of dispersion. This means that for light of a given wavelength λ, all optical path lengths from the source to the detector must be the same. In addition, the same must hold true for all the wavelengths within the spectrum of the light pulse. To attain these requirements, the mirrors in the grating spectrometer have to be spherical so that by imaging the grating into itself, the spectral dispersion introduced by the grating can be eliminated. The method resembles the zero-dispersion pulse compressor arrangement used for shaping femtosecond laser pulses [17]. The details of the technique are the focus of this article and the analysis of the optical configuration as given in Sect. 5 constitutes the main results.

The isolation of a single harmonic or a group of harmonics without substantially altering their duration has also been proposed in a scheme described in [18]. It includes two reflection gratings in an arrangement in which one grating compensates for the dispersion introduced by the other. Also, a simple dispersionless auto-correlator utilizing a focusing mirror split into two halves has been reported in [19]. The scheme, however, does not allow for a selection of a group of harmonics and it auto-correlates two different cross-sectional parts of the XUV beam, thus presuming transverse coherence.

3 Properties of the free-standing transmission grating

As is schematically shown in Fig. 2a, the free-standing transmission grating consists of equidistantly arranged parallel bars usually made of gold. The parameters characterizing the grating are the grating constant d, which corresponds to the spatial periodicity of the structure, and the width of the gap between bars a. The cross section of the individual bars is usually close to quadratic so that their thickness is approximately $\sim d - a$. The commercially available gratings have 1000–5000 ℓ/mm, which corresponds to a grating constant of $d = 0.2$–1 μm. Despite their fragility, these gratings can be made to cover large areas with a diameter of > 10 mm. To reinforce the fine structure, a coarser grid is used with thicker bars. The periodicity of the coarser structure is usually > 30 d so that its contribution to the dispersion of the

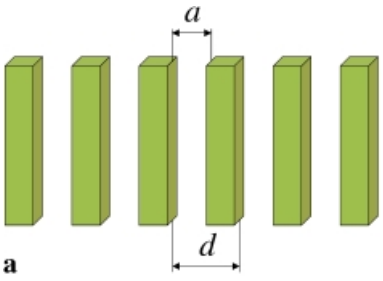

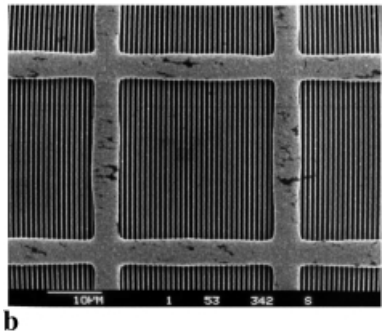

FIGURE 2 **a** The one-dimensional free-standing transmission grating consists of thin gold wires with close to square cross section. They are equidistantly spaced with periodicity d. The space between wires is a. **b** Scanning electron microscope picture of a 1000-ℓ/mm transmission grating manufactured by Heidenhain GmbH [20]

incident radiation is negligible. An example of such a grating fabricated by Heidenhain GmbH [20] is shown in Fig. 2b.

An important feature of these gratings, which is of primary importance to the application envisaged here, is their flat spectral response. In the case of completely opaque bars, Kirchhoff's diffraction theory gives the following expression for the mth-order efficiency, defined as the ratio of the energy contained in the mth order to the total energy incident on the grating [21, 22]:

$$\eta_m = \left(\frac{a}{d}\right)^2 \left[\frac{\sin\left(m\pi\frac{a}{d}\right)}{m\pi\frac{a}{d}}\right]^2, \quad m = 0,\ 1,\ 2, \ldots . \tag{1}$$

In contrast to the reflection gratings, the efficiency of the transmission grating is a function of the ratio a/d only and therefore independent of the wavelength. From (1), it is seen that for a gap-to-grating-constant ratio of $a/d = 0.5$, the grating exhibits the maximum efficiency into the first order of $\eta_1 = 1/\pi^2 \approx 10\%$, whereas 25% of the energy goes into the zeroth order ($\eta_0 = 0.25$). Assuming no losses from the mirrors, after a double passage of the beam on either the zeroth–first-order or the first–zeroth-order arm through the grating, the overall efficiency would be 2.5%.

The efficiency of the grating is given by (1) over a broad spectral range. The short-wavelength limit is due to the fact that eventually the gold bars become partially transparent to the incoming radiation, thus rendering the pure amplitude grating into a phase grating. This depends on the bar thickness and material and, for a 1000 ℓ/mm gold grating, occurs at about $\lambda = 10$ nm (see [21, 22]). The long-wavelength limit is for $\lambda \sim a$, where transmission resonances appear and the efficiency becomes strongly wavelength-dependent [23]. Hence, for a 1000-ℓ/mm gold transmission grating, the wavelength range of applicability as a pure amplitude grating is from 10 nm to about 100 nm. For a Ti:sapphire laser, this corresponds to a range between the fifth and the 80th harmonics of the fundamental frequency. In addition, the simple form of the transmission gratings provides easy alignment and large collection angles.

4 The dispersionless arrangement

In ultra-short-pulse generation, gratings are routinely employed as spectral dispersive elements in pulse-shaping techniques where the sign of group-delay dispersion can be appropriately controlled to stretch or compress a chirped pulse. Gratings are also used in the complementary technique of optical waveform synthesis by means of which a femtosecond pulse can be manipulated to the user's specifications [17]. In the latter scheme shown schematically in Fig. 3a, a zero-dispersion pulse compressor is used in a such a way that the output pulse is identical with the input pulse in the absence of a pulse-shaping mask. This is accomplished by setting up the lenses as a unit telescope in a 4-f arrangement and positioning each grating at the conjugate image plane of the other. The mask acting as a spatial light modulator is positioned at the Fourier plane at the middle of the setup.

Figure 3 depicts the transition from a zero-dispersion pulse compressor to a zero-dispersion Michelson interferometer. Instead of a telescope, one can obtain a direct image of each grating into the other with unit magnification by using a single lens of the same focal length but positioned at the middle of the setup (see Fig. 3b). The difference from the previous

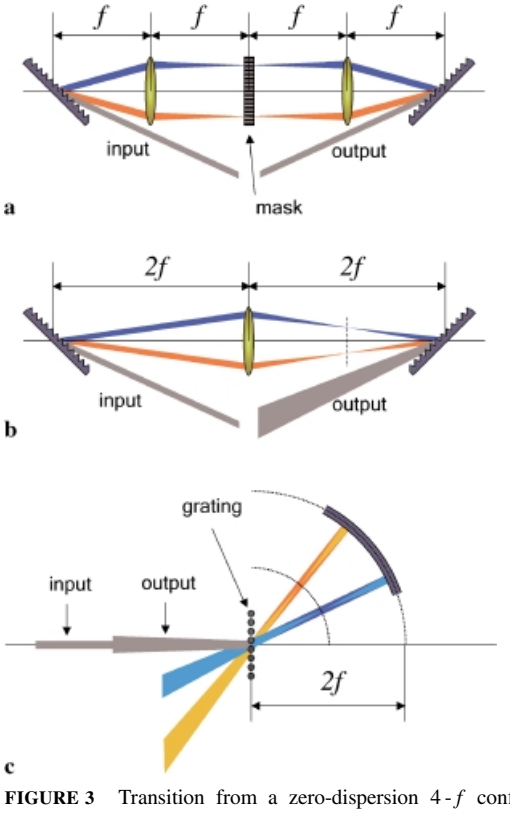

FIGURE 3 Transition from a zero-dispersion 4-f configuration (**a**) to a zero-dispersion arrangement consisting of two reflection gratings and a single lens (**b**) and to a transmission grating plus spherical mirror Michelson interferometer (**c**) where only one arm is shown. In the last setup, the transmission grating takes over the role of the two reflection gratings and the spherical mirrors replace the lens

arrangement is that the Fourier plane is now located midway between the lens and the second grating at the output and the output beam is divergent. There is an additional difference that will be discussed in more detail later on. The pulse at the output has not suffered any dispersion, but the pulse front is now skewed with respect to the propagation direction.

The final step towards a dispersionless Michelson interferometer for the XUV spectral region involves the replacement of the lens by a spherical mirror and of the reflection grating by a free-standing transmission grating. This is schematically shown in Fig. 3c. As can be seen, the grating is located at the geometrical center of the sphere defined by the radius of the spherical mirror. This assures a one-to-one imaging of the grating into itself. While all frequencies combine to form the output beam as in the case of Fig. 3b, there is also the zeroth order of the reflected spectrum that exits the grating and which will be the object of the ray-tracing analysis presented in Sect. 5.

5 The ray-tracing analysis

Although the one-to-one imaging guarantees dispersion-free conditions, the overall performance of the arrangement shown in Fig. 3c depends on several approximations mainly connected with the aberration-free behavior of the spherical mirrors. To assess the influence of these components, we have performed detailed ray-tracing calculations of a specific arrangement of practical importance to the metrology of attosecond pulses. The geometry is shown in Fig. 4 along with the relevant parameters. The inclusion of a third mirror at the exit of the interferometer serves to refocus the divergent beam and also to further image-relay the grating at the detector plane. It introduces some additional freedom with which the arrangement can be adjusted for optimum dispersion or focusing.

The analysis of the arrangement was performed using a simple two-dimensional (2-D) ray-tracing code. For a more realistic three-dimensional (3-D) analysis, we employed the OPTICA package of MATHEMATICA [24]. These calculations deliver more information regarding the pulse-front propagation since they include both dimensions perpendicular to the propagation direction. The most important application of the OPTICA package is, however, the analysis of a true three-dimensional setup which is presented later on.

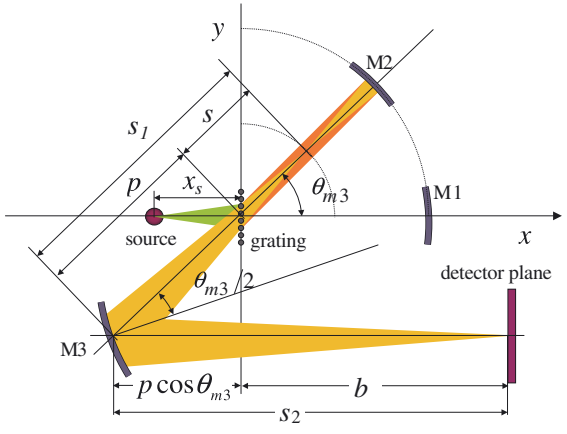

FIGURE 4 The geometry of the grating Michelson interferometer where the coordinate system and the parameters used for the ray-tracing codes are defined. The specific values used for the three cases analyzed are given in Table 1

The basic ingredient in the 2-D code is the grating equation:

$$\sin\theta_{\text{in}} - \sin\theta_{\text{out}} = m N_{\text{g}} \lambda \,, \tag{2}$$

with θ_{in}, θ_{out} the angles with respect to the perpendicular to the grating surface of the incident and diffracted rays, respectively, m the order of diffraction, and $N_{\text{g}} = 1/d$ the number of lines per unit length. The center of the grating opening is chosen to be the origin of the coordinate system used. For a point source located at a distance x_{s} from the grating, a selected number of rays are followed in their propagation through the grating, reflection off the spherical surface of the mirror (M1 or M2), second passage through the grating again, and final reflection off the focusing mirror (M3). A slit of width s_{g} positioned in front of the grating determines the acceptance angle of the setup. The total optical path $l(\omega)$ traveled by each ray of a given frequency is measured at the detector plane located at a distance b from the grating. This analysis is repeated for the two different arms, i.e. the zeroth–first-order arm and the first–zeroth-order arm. All mirrors are specified through their radius $r_{\text{M1,2,3}}$ and the coordinates $x_{\text{M1,2,3}}$ and $y_{\text{M1,2,3}}$ of the center of the sphere of which they comprise a sector.

While the positions of the mirrors M1 and M2 are completely fixed by the requirement that the grating is imaged into itself, the third mirror M3 can be positioned so that a point along the direction of a specific harmonic has its image on the detector plane. If θ_{M3} is the angle of diffraction of the harmonic and f the off-axis focal length of the mirror M3, then the distance $s_1 = p + s$ between object and mirror and the distance $s_2 = p\cos\theta_{\text{M3}} + b$ between mirror and image can be determined by solving for p the following equation:

$$\frac{1}{p+s} + \frac{1}{p\cos\theta_{\text{M3}} + b} = \frac{1}{f} \,. \tag{3}$$

In general, the spherical mirror has two focal lengths as a result of the astigmatism associated with it. The vertical (sagittal) focal length $f_{\text{v}} = r\cos(\theta_{\text{M3}}/2)/2$, which for a parallel beam gives a line focus perpendicular to the plane of incidence. The horizontal (tangential) focal length $f_{\text{h}} = r/[2\cos(\theta_{\text{M3}}/2)]$, which for a parallel beam gives a line focus parallel to the plane of incidence. In this way one can arrange the position of the mirror so that either the horizontal or the vertical focus is on the screen. For $s = 0$, the grating is imaged relayed to the screen.

The path traveled by a light ray through a dispersive system is a function of frequency. This is due to geometrical factors associated with different deflection angles according to wavelength. The phase-advance function $\phi(\omega)$ when expanded to a Taylor series in frequency contains coefficients that are specific to the geometry of the arrangement [13]. Furthermore, it has been shown that the first derivative of the phase with respect to the frequency, the so-called group delay D_1, is exactly given by the relation [25, 26]:

$$D_1 = \frac{\mathrm{d}\phi(\omega)}{\mathrm{d}\omega} = \frac{l(\omega)}{c} \,. \tag{4}$$

Parameter		Case-I	Case-II	Case-III
λ_L	(μm)	0.8	0.8	0.8
N_g	(ℓ/mm)	1000	1000	1000
s_g	(μm)	350	350	350
x_s	(cm)	-20	-20	-20
r_{M1}	(cm)	30	30	30
x_{M1}	(cm)	0	0	0
y_{M1}	(cm)	0	0	0
r_{M2}	(cm)	30	30	30
x_{M2}	(cm)	0	0	0
y_{M2}	(cm)	0	0	0
r_{M3}	(cm)	60	60	60
x_{M3}	(cm)	13.9	20.4	~ 20.0
y_{M3}	(cm)	-0.41	-0.25	~ 0.1
b	(cm)	40	40	~ 38.45
n_1		25	25	25
n_2		37	37	39
n_{hc}		31	31	31
θ_{M3}	(deg)	1.47	1.47	1.47
s	(cm)	0	8.57	~ 8.57
s_1	(cm)	46	48.1	~ 48.57
s_2	(cm)	86	79.5	~ 78.45
h	(mm)	0	0	1, 3, 5
D_2	(fs^2)	$< 1.0^{-3}$	< 1.0	$< 1.2 \times 10^{-3}$

TABLE 1 The parameters of the three cases investigated using the ray-tracing codes. The origin of the coordinate system is located at the middle of the grating aperture (see Fig. 4)

For a specific arrangement, once the optical path l as a function of frequency has been determined, the group-delay dispersion D_2 that describes the temporal broadening of a short pulse traveling through this arrangement is given by [27]:

$$D_2 = \frac{\mathrm{d}^2\phi(\omega)}{\mathrm{d}\omega^2} = \frac{1}{c}\frac{\mathrm{d}l(\omega)}{\mathrm{d}\omega}, \tag{5}$$

whereas the corresponding phase variation as a function of frequency can be obtained from:

$$D_0 = \phi(\omega) = \frac{1}{c}\int_{\omega_0}^{\omega} l(\omega')\mathrm{d}\omega' + \phi_0. \tag{6}$$

The latter quantity can be used for reconstructing the exact temporal shape of the pulse upon exiting the system.

In what follows, we present the results of the ray-tracing simulations for three specific arrangements involving a transmission grating and three spherical mirrors. All the arrangements under consideration are designed and analyzed from the point of view of appropriateness for the investigation of attosecond pulses resulting from the synthesis of a number of phase-locked harmonics like those produced from atomic gas. The values of the parameters that define each arrangement in the way shown in Fig. 4 are given in Table 1.

5.1 *Ray tracing: case-I*

In this arrangement, the two spherical mirrors M1 and M2 have their centers at the middle of the grating and the focusing mirror M3 is positioned in a such a way so that the grating is imaged into the screen. This position is found from (3) with $s = 0$. The results of the ray-tracing codes are summarized in the left column of Fig. 5. We have considered a source emitting odd harmonics of the fundamental frequency of a Ti:sapphire laser ($\lambda_L = 0.8\,\mu$m). The grating disperses all harmonics in the first order, but for simplicity we have calculated only the optical paths of harmonics between $n_1 = 25$ and $n_2 = 37$. This can be rather easily accomplished in practice by mechanically obstructing the unwanted harmonics or by aperturing the mirror M3 to include only a specific selection. As central harmonic n_{hc} we have taken the 31st. The dispersion angle of this harmonic as obtained from (2) determines the focal length of the mirror M3 and its position through (3). For a grating with $N_g = 1000\,\ell$/mm, $\theta_{M3} = 1.47°$.

The optical paths of these harmonics for both arms (zero–first and first–zero orders) are given in Fig. 5 a (case-I). It should be pointed out here that due to the different scales used for the x- and y-axes the plot is strongly distorted. Although not discernible in the plot, both arms of each harmonic co-propagate after the second passage through the grating. The ray-tracing code calculates the total length of the optical path for the central ray and for all paraxial but diverging rays. For a given harmonic, the optical path difference at the detector plane of each paraxial ray from the central (chief) ray $\Delta l^{(n)}_{\mathrm{front}} = l^{(n)}_{\mathrm{paraxial}} - l^{(n)}_{\mathrm{chief}}$ yields the tilting of the pulse front. This is depicted in Fig. 5b (case-I) for all harmonics considered. The difference in the arrival times between the central ray and the extreme paraxial ray for each harmonic also at the detector plane $\Delta t^{(n)}_{\mathrm{paraxial}} = \max(l^{(n)}_{\mathrm{paraxial}} - l^{(n)}_{\mathrm{chief}})/c$ is given in Fig. 5c (case-I). As seen from Fig. 5b and c (case-I), in this setup all harmonics have the same pulse-front skewness. The 3-D ray-tracing code confirms this and gives the complete 2-D information regarding the pulse-front surface (see Fig. 5d (case-I)).

The most important information pertaining to the application envisaged for this setup is its dispersive characteristics. Figure 5e (case-I) gives the difference in the arrival times at the screen between the central harmonic ($n_{hc} = 31$) and all other harmonics. Albeit in a discrete form, this is the group delay relative to the 31st harmonic as a function of frequency (see (4)). Using a spline interpolation, a continuous function can be obtained, the derivative of which gives the group-delay dispersion (see (5)). The ray-tracing calculation reveals the very important result that the difference in the arrival times of the various harmonics around the 31st is less than 2 as. Using (5) and for $\omega_L = 2.36\,\mathrm{fs}^{-1}$ ($\lambda = 0.8\,\mu$m), it is found that in this spectral range the arrangement of case-I exhibits a group-delay dispersion of $D_2 < 1\,\mathrm{as}^2$.

Since in an off-axis imaging using a spherical mirror there are two focal lengths, the question arises of which one exhibits the less dispersion. For the off-axis angle of $\theta_{M3}/2 = 0.735°$, the ratio of the two focal lengths is $f_v/f_h = \cos^2(\theta_{M3}/2) \approx 0.999835$. This difference between the two foci is negligibly small; however for path differences in the attosecond time scale, it plays a role. Indeed, the group delay for f_h is a factor of five higher than the one shown in Fig. 5e (case-I), which has been calculated for $f = f_v$.

The advantage in this arrangement is that all harmonics have the same spot size on the screen and they overlap exactly irrespectively of the arm they belong to. Also, it exhibits an extremely low dispersion of the order of an attosecond. This

is considerably less than the one obtained in the compensated grating configuration described in [18]. The spot size is the image of the grating slit and, therefore, it is determined by the magnification factor introduced by the mirror M3. In the example analyzed, the spot size on the screen is about $\sim 650\,\mu$m.

5.2 *Ray tracing: case-II*

The main difference in this case compared to the previous one is that instead of imaging the grating into the screen, we have chosen to image-relay the source (here assumed to be a point source) to the screen. Both mirrors M1 and M2 form an image of the source in the space behind the grating. After diffraction by the grating, the image is also deflected, but for all harmonics lies on a circle with radius $s_{M1} = r_{M1} - v_{M1}$. The length v_{M1} is obtained from the lens equation $1/f_{M1} = 1/v_{M1} + 1/u_{M1}$ with $u_{M1} = r_{M1} - x_s$. Again the 31st harmonic is taken as the central harmonic and the positioning of the mirror M3 is calculated from (3) with $s = s_{M1}$.

In this case, the individual harmonics come to a focus on the screen, but their foci are spatially separated. This is illustrated in Fig. 5a (case-II). Also, the pulse fronts are more

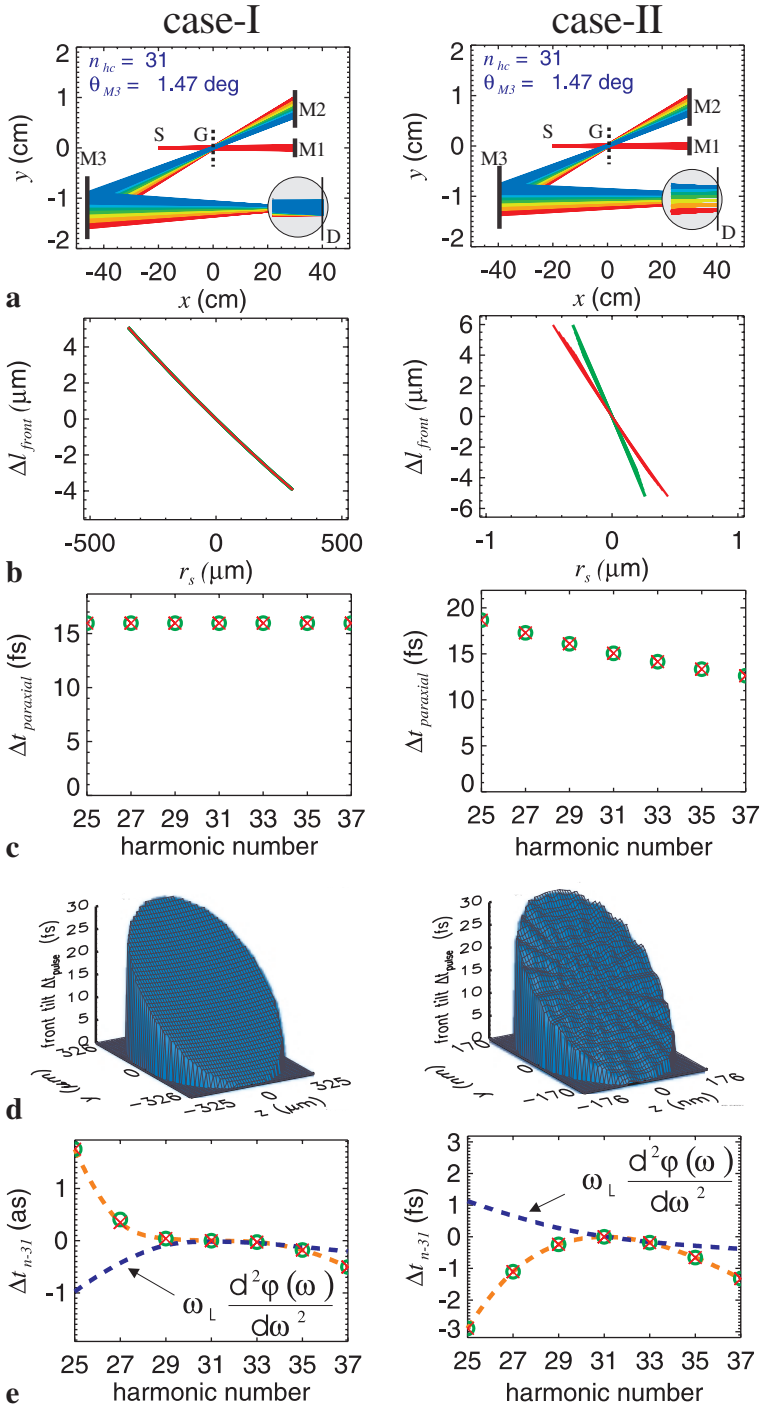

FIGURE 5 Ray-tracing results. Case-I (*left*): the grating is imaged to the detector plane ($s = 0$). Case-II (*right*): the source is image-relayed to the detector plane ($s = 8.57$ cm). **a** Optical paths of the harmonics between $n_1 = 25$ and $n_2 = 37$ for both arms (zero–first and first–zero orders). The exact geometry and the parameters are shown in Fig. 4 while their values are given in Table 1. The source is denoted by S, the grating by G and the mirrors by M1, M2, M3. In the *inset*, a magnification is shown of the image of the source for each harmonic at the detector plane D. **b** Pulse-front tilting as a function of the spot radius r_s for all harmonics in both arms. In case-II, the *dark lines* represent the pulse front of the harmonics from the first–zero-order arm, while the *light lines* are from the zero–first-order arm. In case-I, all harmonic pulse fronts in both arms coincide. **c** The difference in arrival times between the chief ray and the extreme paraxial ray for the harmonics $n = 25$–37. The symbols denote the two arms (*circle*: zero–first, *cross*: first–zero). **d** The pulse front for the central harmonic $n_{hc} = 31$ at the detector plane as calculated with the OPTICA package. The modulation in case-II is due to numerical artifacts. **e** *Points*: the group delay relative to the 31st harmonic $D_1(\omega) = [l_n(\omega) - l_{31}(\omega)]/c$ for the harmonics $n = 25$–37. The symbols denote the two arms (*circle*: zero–first, *cross*: first–zero). *Dark dashed line*: the group-delay dispersion obtained by differentiation of the smooth spline-interpolation (*light dashed line*) for the group delay

severely tilted than in case-I and the tilt for the two arms is slightly different (see Fig. 5b (case-II)). Furthermore, the tilt decreases with the harmonic number (Fig. 5c (case-II)). The spot size is about 0.35 μm and due to the astigmatism introduced by the mirror M3 considerably greater than the diffraction-limited spot for the harmonic wavelength of $\lambda_{31} = 0.8/31 = 0.026$ μm. It should be mentioned here that the modulation observed on the pulse-front surface of Fig. 5d (case-II) is due to numerical artifacts.

As expected, since the grating is not image-relayed to the screen, this setup is not as dispersion-free as that studied in case-I. Despite that, as can be seen from Fig. 5e (case-II), the dispersion introduced is still quite low and acceptable for measuring femtosecond pulses.

5.3 *Ray tracing: case-III*

A novel arrangement that combines the advantages of the two cases already presented and is similarly based on a transmission grating and spherical mirrors is shown in Fig. 6. Unlike the previous two cases, this arrangement is a 3-D setup and therefore only the OPTICA package with 3-D capabilities can be used to assess the effect of aberrations.

Co-propagating fundamental and harmonic beams produced in a non-linear medium (NLM-1, e.g. gas jet) impinge on the free-standing transmission grating G (Fig. 6). The zeroth order passes straight through while the beam diffracted in one of the first orders disperses, resulting in well-separated harmonic beams. In this way, a frequency range corresponding to a set of harmonics can readily be selected using an iris or appropriate obstacles. As in the setups discussed already, the two spherical mirrors (M1 and M2) are used to redirect the selected spectral range as well as the zeroth order back through the grating. These two mirrors are positioned so that they image the grating into itself. In contrast to the previous schemes, they are slightly tilted so that the back-reflected beams are somewhat elevated in the vertical plane and thus spatially separated by the elevation height h from the incoming beam. In addition, the efficiency associated with the two arms is not the same since one arm comprises the zeroth–zeroth-order path and the other the first–first-order path. As a consequence the overall efficiency for the first–first-order path is $\sim 1\%$.

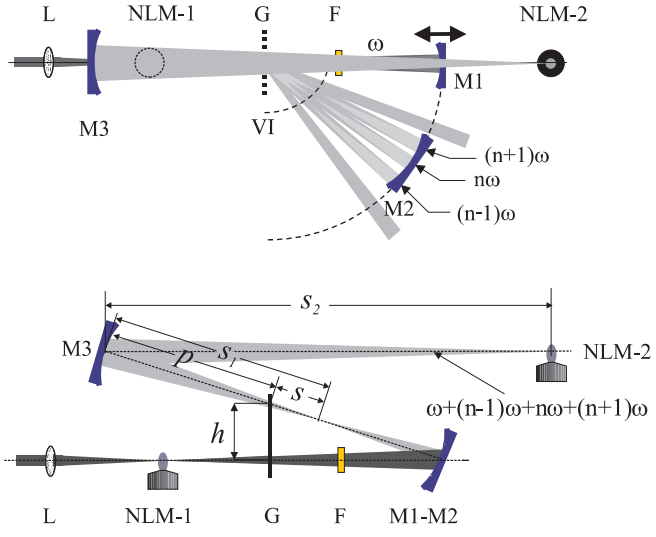

FIGURE 6 Schematic showing the setup analyzed in case-III. *Top*: top view. *Bottom*: side view. The slight tilting of mirrors M1, M2, M3 gives rise to an elevation h at the grating G between incident and back-reflected beams, thus allowing the co-propagation of the two arms after mirror M3. Each one of the dispersed harmonics forms an image of the interaction region NLM-1 that lies on the circumference of a circle VI with center at the middle of the grating. This image is further relayed to a second interaction region NLM-2 where a cross-correlation process takes place. By appropriately aperturing mirror M2 a selection of harmonics can be accomplished. The harmonics are filtered out from the zeroth order by means of a filter F

The between-image of the interaction region is different for each harmonic but, as already mentioned, it is located on a concentric circle with the circle corresponding to mirrors M1 and M2 and with radius $< r_{M2}/2$. Upon exiting the grating all the first orders of the selected harmonics become co-propagating with the back-reflected zeroth order of the fundamental. Finally, a third mirror (M3) further directs and focuses the harmonic mixture and the fundamental to a second non-linear medium (NLM-2). This last mirror relays the between-image of the interaction region in the primary non-linear medium into a secondary non-linear medium. A simple inspection of the geometrical arrangement immediately reveals that in the 2-D geometry the setup is strictly dispersionless. All harmonics and the fundamental travel exactly the same optical path. Furthermore, the harmonic source in the primary non-linear medium is image-relayed to the secondary one after a spectral selection has taken place. Consequently, both requirements of low dispersion and focusing are satisfied simultaneously in this layout.

The 3-D ray-tracing code is of particular importance now in analyzing this setup since it can account for the effect of the mirror tilt on the dispersion and focusing characteristics. The ray-tracing results are summarized in Fig. 7 and in Fig. 8, where for three different values of the elevation h, the front tilt (Fig. 8a), the group delay (Fig. 8b), and the group-delay dispersion (Fig. 8c) for the harmonics $n_1 = 25$ to $n_2 = 39$ are shown. It is seen that even an elevation of $h = 5$ mm for the outgoing beam above the incoming beam at the grating results in a negligible deviation from the strictly dispersionless setup.

The pulse-front tilting is < 10 as for all the harmonics between the 25th and the 37th (see Fig. 8a) with decreasing tendency towards higher harmonics. More importantly, the group-delay dispersion D_2 is of the order of ~ 1 as^2 (see

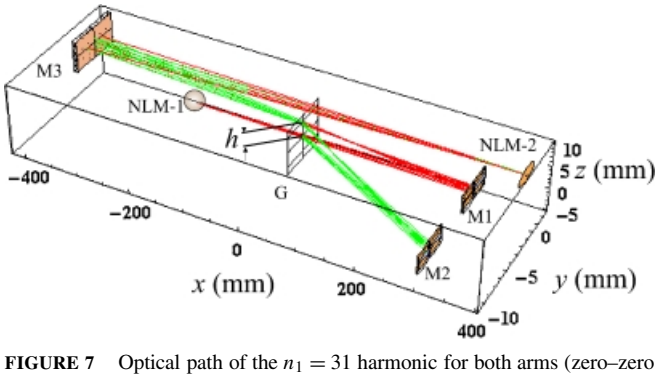

FIGURE 7 Optical path of the $n_1 = 31$ harmonic for both arms (zero–zero and first–first orders). The geometry is shown in Fig. 6, whereas values of pertinent parameters are given in Table 1

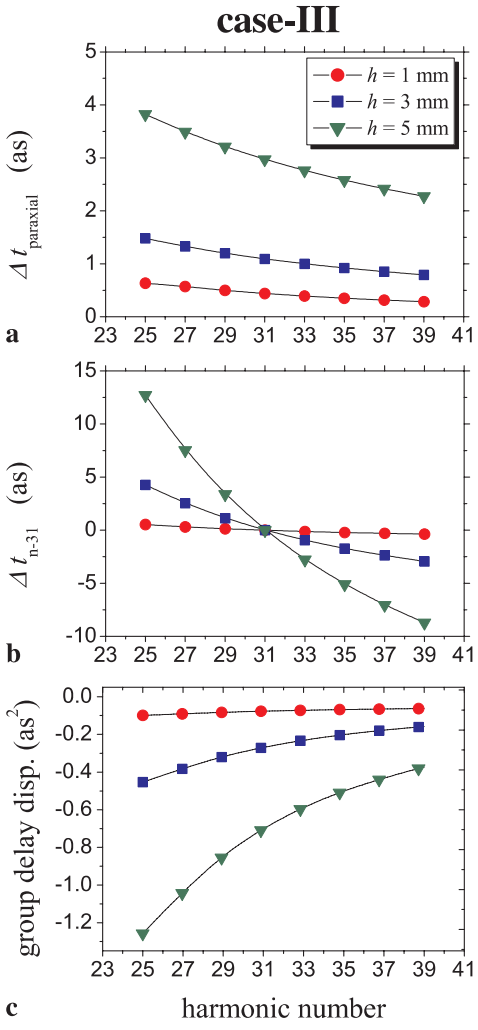

FIGURE 8 Ray-tracing results for case-III with the indicated values for the elevation h and for the harmonics $n = 25$–39. **a** The difference in arrival times between the chief ray and the extreme paraxial ray. **b** The group delay. **c** The group-delay dispersion obtained by differentiation of the smooth spline-interpolation for the group delay (*solid line* in **b**)

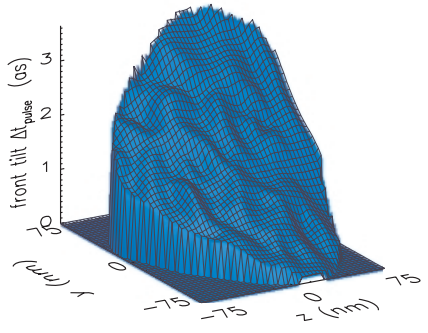

FIGURE 9 The pulse front for the central harmonic $n_{hc} = 31$ and for an elevation $h = 3$ mm at the detector plane as calculated with the OPTICA package. The observed modulation is due to numerical artifacts

Fig. 8c), which makes this arrangement especially suited for attosecond-pulse metrology. The spot size given in Fig. 9 approaches the diffraction-limited one corresponding to the wavelength for the 31st harmonic $\lambda_{31} = 0.8/31 = 0.026\,\mu$m. As the calculation is close to the limit of the numerical accuracy that one can expect from the results, the structure seen on the spot pulse front could be due to numerical uncertainties. Besides, the geometrical abberations may not be dominant in this case in determining the spot size, as diffraction effects may play a role.

6 Discussion and efficiency estimates

In the time domain, the superposition of a group of phase-locked harmonics possessing approximately the same amplitude leads to a train of sharp spikes at intervals of $T_L/2 = \pi/\omega_L$, i.e. half the laser period. The duration of each spike depends on the number of harmonics involved and the degree of chirp in each harmonic. For transform-limited harmonics, each spike has a duration of $\approx T_L/(2N_h)$, where N_h is the number of harmonics in the superposition. More specifically, the case we have considered in the ray-tracing analysis consists of a group of seven harmonics of the Ti:sapphire laser fundamental frequency centered around the 31st. Given that $T_L = 2.67$ fs, this would result in a train of successive spikes with full width at half maximum $\Delta T \simeq 190$ as. In the following, we discuss the suitability of each of the setups we have analyzed in experimentally investigating the characteristics of this pulse train.

The setup discussed in case-I is ideally suited for first-order (field) auto-correlation measurements of a group of harmonics or of a single harmonic. In this case, at the detector plane a linear detector would produce a signal proportional to:

$$S_E(\tau) = \int_{-\infty}^{+\infty} |E_{\rm tot}(t) + E_{\rm tot}(t-\tau)|^2 {\rm d}t,$$

where $E_{\rm tot}$ is the total electric field and τ the relative delay between the two arms of the grating Michelson interferometer. This type of measurement reveals the spectrum of the harmonic superposition and its temporal coherence length. Only if one knows beforehand that all harmonics are transform-limited, the duration of each spike can be deduced.

The duration of a single harmonic can in principle be measured using the setup studied in case-II. As has already been discussed, each harmonic pair from the two arms after the second passage through the grating is co-propagating and focused in a spatially separated point at the detector plane. By isolating a single harmonic E_{ω_n} through proper apertures and assuming that a two-photon detector with enough sensitivity is available, the interferometric auto-correlation trace

$$S_{\rm if}(\tau) = \int_{-\infty}^{+\infty} \left| \left[E_{\omega_n}(t) + E_{\omega_n}(t-\tau) \right]^2 \right|^2 {\rm d}t$$

or the intensity auto-correlation trace

$$S_{\rm I}(\tau) = 1 + 2 \int_{-\infty}^{+\infty} \left[E_{\omega_n}(t) E_{\omega_n}(t-\tau) \right]^2 {\rm d}t$$

can be obtained.

In conjunction with this application two factors have to be considered. The first factor is the requirement of low dispersion. This can be satisfied if the mirror M3 is adjusted so

that the harmonic under investigation becomes the central harmonic. In this case and for a spectral range around the central harmonic, the group-delay dispersion attains values close to zero because the group delay exhibits a local maximum there (see Fig. 5e (case-II)). The second factor is the harmonic focal intensity, which depends on the overall efficiency of the setup. In addition to the double-pass efficiency of the grating $\eta_g \simeq 0.025$ (see 3), the reflectivity of the gold mirrors has to be taken into consideration. For a perpendicular angle of incidence and in the spectral range of 50–100 nm, gold mirrors have a reflectivity of $R_m \simeq 10\%$. Therefore, after reflection off mirrors M1, M2, and M3, the overall efficiency of the setup is estimated to be $\eta_{tot} \simeq 2.5 \times 10^{-4}$. A second-order auto-correlation measurement of the ninth harmonic from Xe gas has been reported in [28], where two-photon ionization of He was used as a non-linear process. In this experiment, the focal intensity for the ninth harmonic was estimated to be $I_9 \sim 0.15 \times 10^{12}\,\mathrm{W/cm^2}$. More recently, two- and three-photon ionization of rare gases using the fifth harmonic of a Ti:sapphire laser with an estimated $I_5 \sim 0.4 \times 10^{12}\,\mathrm{W/cm^2}$ has been reported [29]. If we assume that using the arrangement of case-II the ninth harmonic can be isolated and focused to a spot size of the order of the harmonic wavelength $\lambda_9 = 0.8/9 \approx 0.1\,\mu\mathrm{m}$, then the harmonic power required is $P_9 \simeq 47\,\mathrm{W}$. This appears feasible since the ray-tracing analysis of case-II shows that the aberration-limited focal spot is also $\approx 0.1\,\mu\mathrm{m}$ (see Fig. 8b and c (case-II)). For a laser and harmonic pulse duration of $\tau_L = 60\,\mathrm{fs}$ and $\tau_9 \approx \tau_L/\sqrt{9} = 20\,\mathrm{fs}$ respectively, the energy content of the ninth harmonic should then be $E_9^{(out)} \simeq 1\,\mathrm{pJ}$ after the interferometer and $E_9^{(in)} = E_9^{(out)}, /\eta_{tot} \simeq 4\,\mathrm{nJ}$ before it. Presuming a quite plausible fundamental to harmonic conversion efficiency of $\sim 10^{-6}$–10^{-7}, this harmonic energy can be readily delivered by a Ti:sapphire laser system with few mW power output.

The fact that the sensitivity of the non-linear processes drops rapidly for shorter wavelengths renders the method of auto-correlation as not viable for measuring the duration of harmonics or a group of harmonics in the XUV region. The alternative approach for characterizing higher harmonics is then cross-correlation techniques with the fundamental [8, 9, 14]. The arrangement analyzed in case-III has been conceived primarily with this application in mind [14] and it possesses all the necessary prerequisites. For example, the fundamental and harmonic beams are co-propagating (see Fig. 6), the primary interaction region is image-relayed to a secondary one, it exhibits attosecond group delay (see Fig. 8), and it can be appropriately configured to select desired spectral regions. Furthermore, a filter F positioned in the pathway of the zeroth order eliminates all the harmonic radiation in the zeroth-order arm while it attenuates to a desirable degree the fundamental. An appropriate micro-positioning device on which mirror M1 is mounted allows for temporal delay variation between the fundamental and the harmonics. An alternative approach to achieve the same variation would be to insert in the path of the fundamental a glass plate of appropriate thickness which can be accurately rotated. Thus, the harmonic generation (or ionization) signal produced from the interaction of the combined beams with the secondary non-linear medium NLM-2 can be monitored as a function of the delay of the fundamental. As has been discussed in detail in [14], this signal when properly analyzed contains enough information to give the relative phases of the harmonics with respect to the fundamental even in the presence of harmonic chirp.

To estimate the magnitude of harmonic intensities needed in order to perform such a cross-correlation measurement, we consider a seven-photon ionization of an atom by the fundamental vs its single-photon ionization by the seventh harmonic. Since the available fundamental intensity is high (say $10^{16}\,\mathrm{W/cm^2}$), no considerations will be made about the signal produced by it. Even after all losses, the fundamental will be strong enough to almost saturate the ionization process. Then its intensity will have to be reduced in order to make the two ionization amplitudes equal. For the seventh harmonic, we assume a single-photon ionization cross section $\sigma = 10^{-18}\,\mathrm{cm^2}$, a harmonic pulse duration $\tau_7 = 10\,\mathrm{fs}$, an interaction volume $V = 10^{-12}\,\mathrm{m^3}$, and an atomic density $\varrho = 10^{24}\,\mathrm{m^{-3}}$. We require production of $N = 10$ ions per laser pulse, in order to have a well-observable signal. For the numbers given above, a harmonic intensity of $10^3\,\mathrm{W/cm^2}$ at the interaction volume would be sufficient. Assuming four orders of magnitude overall losses at the grating and the mirrors, a harmonic intensity of $10^7\,(\mathrm{W/cm})^2$ at the generation focus is required. This is equivalent to a reasonable fundamental to harmonic conversion efficiency of about 10^{-7}.

Although these estimates suggest that it would be possible to perform auto- or cross-correlation measurements under realistic conditions, the overall efficiency of the grating Michelson interferometer can be increased if necessary. A factor of ~ 100 can be gained if instead of perpendicular, grazing-incidence optics is utilized. An envisaged setup comprises an elliptical mirror with two identical gratings positioned at its foci. For a large enough eccentricity of the elliptical surface, the rays diffracted in the first order by the first grating are focused under a grazing angle into the second one. The zeroth and first orders are thus recombined and after exiting the second grating they co-propagate. This arrangement needs to be assessed with respect to the effect of the geometrical aberrations and it is currently under study.

A critical requirement for the successful application of the method is the high surface quality of the mirrors M1 and M2 and to a lesser extent of the mirror M3. As in a conventional optical interferometer, low surface quality would lead to low contrast fringes while a high degree of microroughness leads to excessive scattering losses. The tolerances with respect to the surface accuracy (deviation from the perfect geometrical shape) of the mirrors depends on the order of the harmonics under investigation. For lower harmonics, mirrors possessing high optical quality in the visible part of the spectrum, e.g. $\lambda/20$–$\lambda/50$ at 632.8 nm, can be readily obtained and they would be of acceptable quality for the investigation of fifth to the 15th harmonic of the Ti:sapphire laser wavelength. For higher harmonics, high-precision optical components should be used of the quality employed in synchrotron radiation sources. The fabrication of a 50-mm-diameter spherical mirror with surface accuracy of $\lambda/10$ at 50.0 nm and a microroughness of 5 Å for a spatial frequency of $1\,\mathrm{mm^{-1}}$ is well within the feasibility limits of today's technology [30].

ACKNOWLEDGEMENTS This work has been performed within the framework of the European Community's Human Potential Programme under Contract No. HPRN-2000-00133, ATTO and it has been partially carried out in the Ultraviolet Laser Facility (ULF) (Contract No. HPRI-1999-CT-00074). One of us (E.G.) acknowledges support by the EPEAEK programme of the Greek Ministry of Education. The authors express their appreciation to J. Flieser and M. Dreher for reading the manuscript and making useful suggestions. G. Tsakiris thanks P. Predehl for useful information on the properties of self-supporting transmission gratings.

REFERENCES

1 G. Farkas, C. Tóth: Phys. Lett. A **168**, 447 (1992)
2 S.E. Harris, J.J. Macklin, T.W. Hänsch: Opt. Commun. **100**, 487 (1993)
3 P. Antoine, A. L'Huillier, M. Lewenstein: Phys. Rev. Lett. **77**, 1234 (1996)
4 M. Protopapas, D.G. Lappas, C.H. Keitel, P.L. Knight: Phys. Rev. A **53**, R2933 (1996)
5 I.P. Christov, M.M. Murnane, H.C. Kapteyn: Phys. Rev. Lett. **78**, 1251 (1997)
6 F.L. Kien, K. Midorikawa, A. Suda: Phys. Rev. A **58**, 3311 (1998)
7 N.A. Papadogiannis, B. Witzel, C. Kalpouzos, D. Charalambidis: Phys. Rev. Lett. **83**, 4289 (1999)
8 P.M. Paul, E.S. Toma, P. Breger, G. Mullot, F. Augé, Ph. Balcou, H.G. Muller, P. Agostini: Science **292**, 1689 (2001)
9 M. Drescher, M. Hentschel, R. Kienberger, G. Tempea, C. Spielmann, G.A. Reider, P.B. Corkum, F. Kraus: Science **291**, 1923 (2001)
10 M. Hentschel, R. Kienberger, C. Spielmann, G.A. Reider, N. Milosevic, T. Brabec, P. Corkum, U. Heinzmann, M. Drescher, F. Kraus: Nature **414**, 509 (2001)
11 J.-C. Diels, J.J. Fontaine, I.C. McMichael, F. Simoni: Appl. Opt. **24**, 1270 (1985)
12 J.-C. Diels, W. Rudolph: *Ultrashort Laser Pulse Phenomena* (Academic, San Diego 1996)
13 I. Walmsley, L. Waxer, C. Dorrer: Rev. Sci. Instrum. **72**, 1 (2001)
14 E. Hertz, N.A. Papadogiannis, G. Nersisyan, C. Kalpouzos, T. Halfmann, D. Charalambidis, G.D. Tsakiris: Phys. Rev. A **64**, 051801R (2001)
15 V. Ronchi: Appl. Opt. **3**, 437 (1963)
16 C.R. Munnerlyn: Appl. Opt. **8**, 827 (1969)
17 A.M. Weiner: Rev. Sci. Instrum. **71**, 1929 (2000)
18 P. Villoresi: Appl. Opt. **38**, 6040 (1999)
19 E. Constant, E. Mével, A. Zaïr, V. Bagnoud, F. Salin: J. Phys. IV Fr. **11**, Pr2-537 (2001)
20 Dr. Johannes Heidenhain GmbH, Dr. Johannes Heidenhain Str. 5, 83 301 Traunreut, Germany
(see http: //www.heidenhain.de/e0.htm)
21 H. Bräuninger, P. Predehl, K.P. Beuermann: Appl. Opt. **18**, 368 (1979)
22 K. Eidmann, M. Kühne, P. Müller, G.D. Tsakiris: J. X-ray Sci. Technol. **2**, 259 (1990)
23 H. Lochbihler, R.A. Depine: Opt. Commun. **100**, 231 (1993)
24 Wolfram Research, Inc., 100 Trade Center Drive, Champaign, IL 61820-7237, USA
(see http: //www.wolfram.com)
25 E.B. Treacy: IEEE J. Quantum Electron. **QE-5**, 454 (1969)
26 S.D. Brorson, H.A. Haus: J. Opt. Soc. Am. B **5**, 247 (1988)
27 C.M. González Inchauspe, O.E. Martínez: J. Opt. Soc. Am. B **14**, 2696 (1997)
28 Y. Kobayashi, T. Sekikawa, Y. Nabekawa, S. Watanabe: Opt. Lett. **23**, 64 (1998)
29 D. Descamps, L. Roos, C. Delfin, A. L'Huillier, C.-G. Wahlström: Phys. Rev. A **64**, 031404R (2001)
30 C.J. Walsh, A.J. Leistner, J. Seckold, B.F. Oreb, D.I. Farrant: Appl. Opt. **38**, 2870 (1999)